Controllable parabolic-cylinder optical rogue wave

Wei-Ping Zhong,[1,2,3] Lang Chen,[1,*] Milivoj Belić,[3,4] and Nikola Petrović[4]
[1]*Department of Physics, South University of Science and Technology, Shenzhen 518055, China*
[2]*Department of Electronic and Information Engineering, Shunde Polytechnic, Guangdong Province, Shunde 528300, China*
[3]*Texas A&M University at Qatar, P.O. Box 23874, Doha, Qatar*
[4]*Institute of Physics, University of Belgrade, P.O. Box 57, 11001 Belgrade, Serbia*
(Received 14 May 2014; published 6 October 2014)

We demonstrate controllable parabolic-cylinder optical rogue waves in certain inhomogeneous media. An analytical rogue wave solution of the generalized nonlinear Schrödinger equation with spatially modulated coefficients and an external potential in the form of modulated quadratic potential is obtained by the similarity transformation. Numerical simulations are performed for comparison with the analytical solutions and to confirm the stability of the rogue wave solution obtained. These optical rogue waves are built by the products of parabolic-cylinder functions and the basic rogue wave solution of the standard nonlinear Schrödinger equation. Such rogue waves may appear in different forms, as the hump and paw profiles.

DOI: 10.1103/PhysRevE.90.043201 PACS number(s): 05.45.Yv, 42.65.Tg, 42.65.Sf, 02.30.Ik

I. INTRODUCTION

The $(1+1)$-dimensional (1D) nonlinear Schrödinger equation (NLSE) with constant coefficients is an integrable model which, among many solutions, supports also the ones that reproduce well the qualitative characteristics of rogue waves [1,2]. This equation describes diverse physical systems, such as nonlinear optical fibers [3], Bose-Einstein condensates (BECs) [4], and others. The relevance of the equation for the study of rogue waves was lately established in various experiments carried out in different physical contexts [5,6]. It should be noted that these solutions—specifically, the Peregrine soliton and Akhmediev and Ma breathers—by themselves are not the proper rogue waves but can be used to model them. On the other hand, the two-dimensional (2D) NLSE with constant coefficients and external potentials may also support propagation of different nonlinear wave packets. These wave packets display many new properties [7–9], such as self-compression [7] and the generation of vortex-ring beams [9].

The elucidation of mechanisms underlying the formation and dynamics of rogue waves (also called the freak or extreme waves) is currently subject to fundamental scientific scrutiny. They occur in many fields, such as oceanography [10], nonlinear optics [11], and BECs [4]. A comprehensive recent review of rogue waves can be found in [12,13]. An explicit rogue wave solution of the standard NLSE was derived in 1983 [14]; after the author, the solution was called the Peregrine breather or an algebraic breather. Other related rogue wave solutions of the standard NLSE were found by Ma [15] in 1979; these are solutions that breathe temporally but are localized spatially, for example, along a fiber. Akhmediev found a new kind of solutions, now called Akhmediev breathers [16,17], which were qualitatively different from the Ma breathers. Akhmediev breathers oscillate spatially but are localized in time. In other words, Akhmediev breathers are the exact pulse solutions of the standard NLSE that extend transversely and may arise from the transverse modulation instability of a plane wave [17]. On the other hand, the Peregrine breather is a localized solution in both space and time [14], and can thus be seen as the limit of both the Ma and the Akhmediev breathers.

Recently, the first-order and second-order Peregrine rogue wave solutions—indeed, solutions all the way up to the fifth order—have been observed in a water wave tank [18,19]. Also, rogue waves described by the Peregrine rational solution have been generated in optics [20] and magnetoplasma [21,22]. Thus the validity of the simplest rogue wave solutions has been confirmed experimentally. A direct approach to finding multi-rogue-wave solutions of the standard NLSE, based on the modified Darboux transformation, is presented in [23]. It is worth mentioning that the rogue wave solutions were exhibited in the inhomogeneous NLSE with variable coefficients. Periodic and hyperbolic wave functions may display the dynamical behavior of roguelike wave phenomena. The profiles of the first-order and second-order rogue wave solutions of the inhomogeneous NLSE with variable coefficients can be controlled by a number of parameters [24]. A common characteristic of all these waves is that they ride on a finite background.

In this paper, we demonstrate that a class of parabolic-cylinder optical rogue waves can exist in inhomogeneous media described by the varying coefficients in NLSE. Such solutions, which are constructed by means of the similarity transformation method as products of the parabolic-cylinder function and the basic rogue wave solutions of the standard nonlinear Schrödinger equation, form relatively stable rogue wave patterns while propagating. These controllable profiles of the optical rogue waves can be realized by selecting different orders of the parabolic-cylinder function. Since in general the media exhibiting rogue waves that can be controlled—such as nonlinear optics and BECs—are inhomogeneous and can be better described by the NLSE with varying coefficients, it is expected that the solutions obtained in this paper will have a greater influence on the quest for finding changeable but feasible rogue waves in experimentally controlled environments [12,13].

The paper is organized as follows. In Sec. II, we introduce the generalized nonlinear Schrödinger equation with spatially modulated coefficients and a special external potential, and construct an explicit form of the rogue wave solution of the model through the similarity transformation. We then

*chenlang@sustc.edu.cn

elaborate on the method of deriving parabolic-cylinder rogue waves. In Sec. III, we discuss the patterns of first-order, second-order, and third-order rogue wave solutions mentioned above. Section III is also devoted to a numerical study of two solutions in order to compare our numerical simulations with the analytical predictions, and also to confirm the stability of localized solutions. Finally, Sec. IV presents our conclusions.

II. THE MODEL AND THE SIMILARITY TRANSFORMATION

We consider nonlinear optical systems ruled by the generalized NLSE with spatially modulated coefficients and a special external potential which can be written in the following dimensionless form:

$$i\frac{\partial u}{\partial z}+d(x)\frac{\partial^2 u}{\partial x^2}+2N(z,x)|u|^2u+U(z,x)u=0, \quad (1)$$

where $u(z,x)$ represents the complex optical wave envelope, the beam propagates along the z axis, and x is the transverse coordinate. Here, $d(x)$ is the diffraction coefficient, $N(z,x)$ is the nonlinearity coefficient, and $U(x)$ is the external potential. We choose the potential as $U(x)=d(x)(ax^2+b)$, where a and b are the two real constants to be determined below. Hence, the external potential is just a simple quadratic potential, modulated by the diffraction coefficient. In this manner, we try to stay close to the physically relevant situations, so when $d(x)$ is constant, the equation reduces to the Gross-Pitaevskii equation of BECs with harmonic potential. All of the parameters of the equation can be controlled and manipulated by the choice of medium. The nonlinearity coefficient $N(z,x)$ may possess different expressions in Eq. (1); thus it may include many special cases of nonlinear optics and BECs. When $N(z,x)=N(z)$ and $d(x)=1$ in Eq. (1), we have obtained bright and dark soliton solutions by means of the F-expansion method in [25]; the first-order and the second-order rogue waves were also obtained, and the dynamical behavior of those waves was discussed in our previous work [24]. However, the important controllable behavior of rogue waves in [24] has not been investigated, not even for $N(z,x)=N(x)$, and also the third-order rogue waves have not been analyzed at all. We focus in this paper on spatially localized solutions for which $N(z,x)=N(x)$.

In order to find rogue wave solutions of Eq. (1), we presume a relation between $u(z,x)$ and the solution $V(z,Y)$ of the NLSE with constant coefficients, Eq. (3), by utilizing the similarity transformation,

$$u(z,x)=A(X)V(z,Y), \quad (2)$$

$$i\frac{\partial V}{\partial z}+\frac{\partial^2 V}{\partial Y^2}+2|V|^2V=0, \quad (3)$$

where $A(X)$ is the amplitude, assumed to be a real function. Here we introduce two similarity variables $X=X(x)$ and $Y=Y(x)$ to be determined [26,27]. In general, the rogue wave solutions of Eq. (3) have the following basic structure [1]:

$$V_n(z,Y)=\left[(-1)^n+\frac{G_n(z,Y)+iH_n(z,Y)}{F_n(z,Y)}\right]e^{2iz}, \quad (4)$$

where n (=1,2,3, ...) is a positive integer. The polynomial $F_n(z,Y)$ should have no zeros in the region of interest, to ensure that the solution $V_n(z,Y)$ is finite everywhere. The first-order ($n=1$), going to the third-order ($n=3$) rogue wave solutions of Eq. (3), can be found by the direct integration method (see Appendix A).

Substituting Eq. (2) into Eq. (1) leads to Eq. (3), provided that a system of differential equations for X, Y, and $A(X)$ is satisfied:

$$\frac{2}{A}\frac{\partial A}{\partial X}\frac{\partial X}{\partial x}\frac{\partial Y}{\partial x}+\frac{\partial^2 Y}{\partial x^2}=0, \quad (5a)$$

$$\frac{d}{A}\left[\frac{\partial^2 A}{\partial X^2}\left(\frac{\partial X}{\partial x}\right)^2+\frac{\partial A}{\partial X}\frac{\partial^2 X}{\partial x^2}\right]+U=0, \quad (5b)$$

and the following two relations hold:

$$N(x)=\frac{1}{A^2(x)}, \quad \text{and} \quad d(x)=\int\frac{1}{A^2(x)}dx. \quad (5c)$$

These relations establish a connection of the nonlinearity and diffraction coefficients with the presumed amplitude of the solution in Eq. (2) and thus can be considered as constraint conditions on Eq. (1) for solution by the present similarity transformation method. By assuming the simplest possibility $X=x$, one finds the following relation between Y and A:

$$Y(x)=\int A^{-2}dx, \quad (6a)$$

and a simple differential equation for A:

$$\frac{d^2A}{dx^2}+(ax^2+b)A=0. \quad (6b)$$

Equation (6b) is just the Schrödinger equation for the quadratic potential, with the well-known solutions. It is a linear second-order ordinary differential whose general solution can be expressed in terms of many different special functions. We opt for the ones with clear physical relevance and a convenient parameter that allows an easy classification of solutions. More specifically, if we choose $a=-1/4$ and $b=m+1/2$, where m is a non-negative integer, differential equation (6b) is transformed into the canonical form of the parabolic-cylinder differential equation [28] (PCDE), namely,

$$\frac{d^2A}{dx^2}+\left(m+\frac{1}{2}-\frac{1}{4}x^2\right)A=0. \quad (6c)$$

The general solution to PCDE (6c), found by considering the standard Weber differential equation, is

$$A=k\left[c_1D_m(x)+c_2D_{-m-1}(ix)\right], \quad (6d)$$

where c_1 and c_2 ($c_1c_2>0$) are the two integration constants that should be chosen so as to avoid introducing singularities in $Y(x)$. Here, $D_m(x)$ is the parabolic-cylinder function and $k=\sqrt{1/\sqrt{2\pi}m!}$ is the normalization constant. It should be noted that $A(x)$ is real, although the argument of the second parabolic-cylinder function is complex (see Appendix B). Obviously, when $|x|\to\infty$ for any non-negative integer m, $D_m(x)$ tends to a constant.

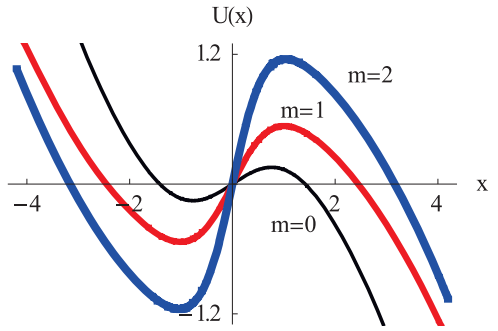

FIG. 1. (Color online) External potential for parameters $c_1 = c_2 = 1$ and different m.

Collecting all these partial solutions together, we obtain an analytical solution of Eq. (1):

$$u(z,x) = \sqrt{\frac{1}{\sqrt{2\pi}m!}}[c_1 D_m(x) + c_2 D_{-m-1}(ix)]V_n(z,Y), \quad (7)$$

which we will refer to as the parabolic-cylinder rogue waves. Since $|u(z,x)|$ vanishes at $|x| \to \infty$, Eq. (7) represents localized wave packets. Here, $Y(x) = k^{-2}\int [c_1 D_m(x) + c_2 D_{-m-1}(ix)]^{-2} dx$ and $V_n(z,Y)$ is defined by Eq. (4). The novel optical rogue waves from Eq. (7) can be conveniently classified by the two integer parameters, n and m. Based on the values of n and m, we can obtain new families of controllable parabolic-cylinder optical rogue waves.

III. CONTROLLABLE ROGUE WAVES

In this section, we consider the cases when m is a nonnegative integer and discuss the profiles of the first-order ($n = 1$), the second-order ($n = 2$), and the third-order ($n = 3$) optical rogue waves. We then check the stability of exact solutions to Eq. (1) as given by Eq. (7) with the quadratic potential coefficient $a = -1/4$, by numerical integration of Eq. (1) with appropriate initial conditions.

A. External potential

When $a = -1/4$ and $b = m + 1/2$, the external potential for different values of parameter m becomes $U_m(x) = \sqrt{2\pi m!}(-\frac{1}{4}x^2 + m + \frac{1}{2})\int \frac{dx}{(c_1 D_m(x) + c_2 D_{-m-1}(ix))^2}$ and is shown Fig. 1. Even though the formula for these optical potentials is complicated, the potential barriers of such form are readily realizable experimentally and theoretically [29,30]. Although the potential includes an explicit quadratic dependence, upon modulation it resembles more a cubic polynomial function. An external potential of this form can serve as an anharmonic trapping potential in BECs that includes a tunneling mechanism; one should keep in mind that interest in the field of BECs is mostly confined to harmonic and liner potentials [30,31]. Additionally, anharmonic potentials may arise in the dynamics of waveguides with specially crafted transverse profiles of the refractive index [32]. A discussion of the influence of polynomial external potentials on NLSE is provided in [33]. Our interest here is confined to providing exact rogue wave solutions to the generalized NLSE that ride on complicated-looking external potentials which display benign-looking profiles. Note that the parameter m is connected with the potential, while the parameter n is connected with the order of the rogue wave solution.

In general, we have a large degree of freedom in choosing n and m. However, when n is greater than 3, $V_n(z,x)$ in Eq. (4) becomes quite complex. Thus, in this paper we only study low-order rogue wave packets. We present the optical amplitude $[I_n(z,x) = \sqrt{|u(z,x)|^2}]$ distributions and their contour plots for specific values of the two parameters n and m. Clearly, the optical intensity can be manipulated by the choice of parabolic-cylinder functions and the order of rogue wave solutions.

B. First-order rogue waves

The simplest case in this family of optical rogue wave solutions given by Eq. (7) is obtained when $n = 1$. In Fig. 2, analytical solutions of the first-order ($n = 1$) rogue waves

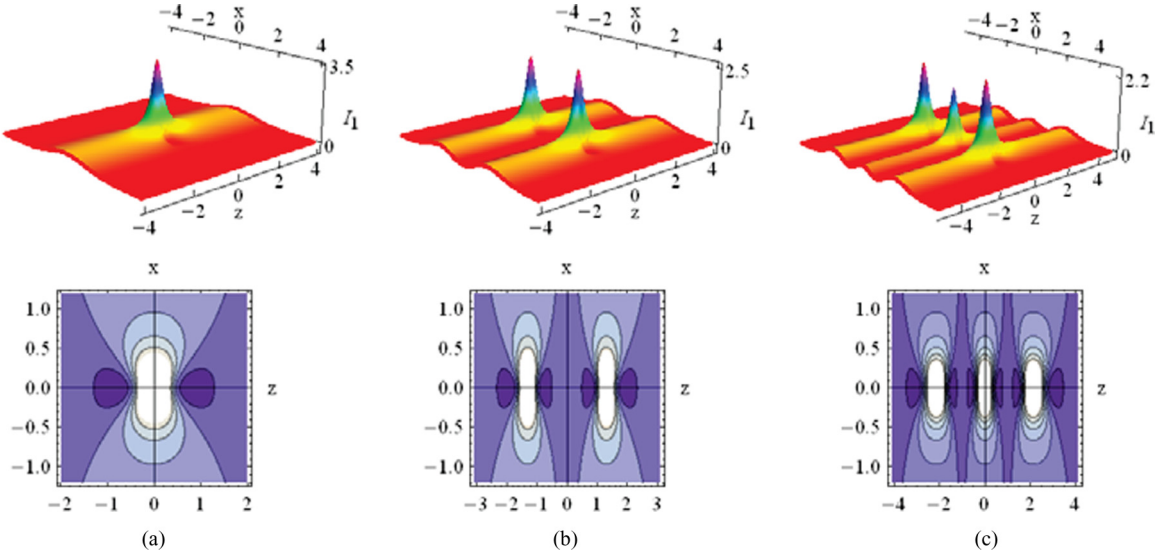

FIG. 2. (Color online) First-order rogue waves with $n = 1$, shown for $m = 0,1,2$ from left to right. Top row shows the intensity distributions, the bottom row the corresponding contour plots.

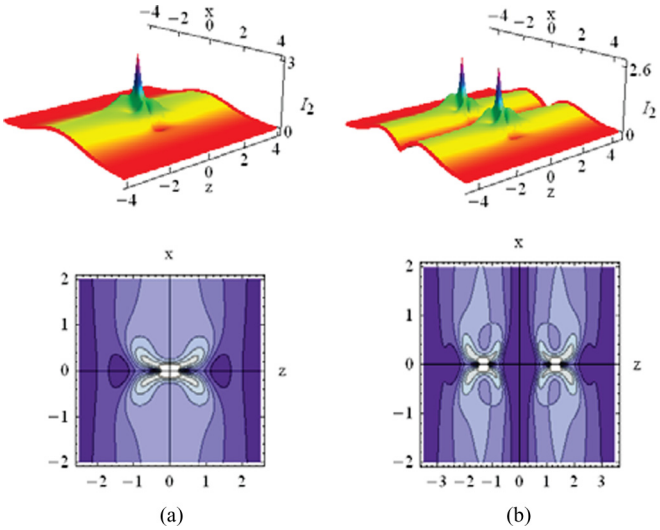

(a) (b)

FIG. 3. (Color online) Profiles of the fundamental second-order rogue waves with the parameters $\alpha_1 = \beta_1 = 0$: (a) $m = 0$ and (b) $m = 1$.

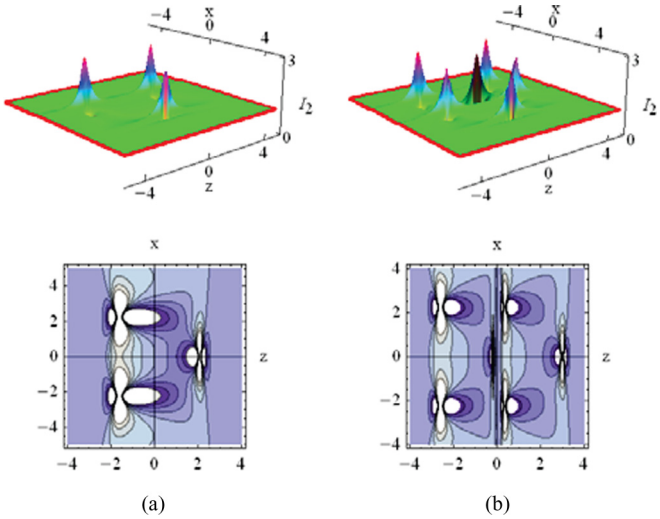

(a) (b)

FIG. 4. (Color online) Multiple four-claw structures for the second-order rogue waves with the parameters $\alpha_1 = 0$, $\beta_1 = -10$: (a) $m = 0$ and (b) $m = 1$. The setup is as in Fig. 3.

are depicted for different m with two integral constants: $c_1 = c_2 = 1$. For simplicity, we keep the constants $c_1 = c_2 = 1$ throughout. Figure 2(a) depicts the distribution when $m = 0$; the profile displays a single peak with two dips. The peak is located at $(z,x) = (0,0)$ and there are two transverse valleys around the peak, akin to the Peregrine soliton. By increasing m to 1, the localized structure with two humps is generated, as in Fig. 2(b). Next, when $m = 2$, Fig. 2(c) shows three profiles for this localized wave packet. We can see from Fig. 2(c) that the smaller hump appears at the central position, while the maximum value is attained at the peaks of the two side humps. In general, for the parabolic-cylinder rogue wave with different m, we find $m + 1$ humps. Furthermore, we find that for even m there is a hump at the central position, which is the smallest, and $m/2$ additional humps on each side of the central position, whereas for odd m there is no hump at the central position.

C. Second-order rogue waves

For $n = 2$, there exist two types of parabolic-cylinder rogue wave families, namely, the fundamental rogue waves with the parameters $\alpha_1 = \beta_1 = 0$ and the excited rogue waves with the real parameters α_1 and β_1, of which at least one is not zero. The second-order parabolic-cylinder rogue waves exhibit pawlike patterns, with "four-claw" symmetrical structures around the central peak. Figure 3(a) shows the intensity of these wave packets for $m = 0$. For $m = 1$, these rogue waves form more complex structures. Two four-claw profiles along the transverse direction are seen in Fig. 3(b).

Another case is obtained for parameters $\alpha_1 = 0$ and $\beta_1 = -10$. Figure 4(a) depicts a typical example in which three similar peaks are located at the vertices of an equilateral triangle, for $m = 0$. For $m = 1$, the pattern of the rogue wave displays six four-claw structures, as seen in Fig. 4(b).

D. Third-order rogue waves

To describe their form, the general third-order rogue wave necessitates four real parameters, α_1, β_1, α_2, and β_2. Therefore the third-order rogue wave displays a more complex structure than the second-order wave. The choice of four parameters can be made in many ways, but we consider the three special cases. In the first case $\alpha_1 = \alpha_2 = \beta_1 = \beta_2 = 0$, which describes the fundamental third-order rogue wave. The remaining two cases are given by $\beta_1 = \beta_2 = 0$, and $\alpha_1 \neq 0$, $\alpha_2 \neq 0$ and by $\alpha_1 = \alpha_2 = 0$, and $\beta_1 \neq 0$, $\beta_2 \neq 0$. In general, we find that many different profiles of rogue waves can be obtained by different combinations of these four parameters.

First, we construct the fundamental third-order rogue wave for $\alpha_1 = \alpha_2 = \beta_1 = \beta_2 = 0$. For $m = 0$ there exist two valleys and a high peak surrounded by six small claws, as seen in Fig. 5(a). Note that the peak is located at the origin $(z,x) = (0,0)$. Figure 5(b) illustrates the rogue wave for $m = 2$. There now exist three "six-claw" patterns, and the intensity is smaller at the central peak than at the two side peaks.

Next, we consider the parameters $\beta_1 = \beta_2 = 0$, $\alpha_1 = \alpha_2 = 50$, and $m = 0$. Figure 6(a) exhibits the second-order

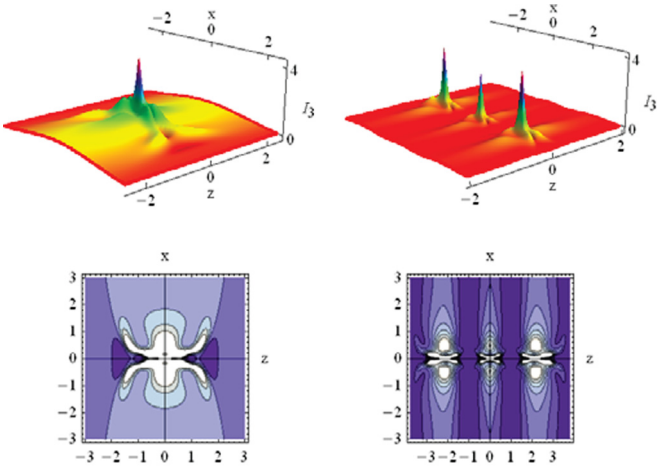

(a) (b)

FIG. 5. (Color online) Intensity of the fundamental third-order rogue waves: (a) $m = 0$ and (b) $m = 2$. The setup is as in Fig. 3.

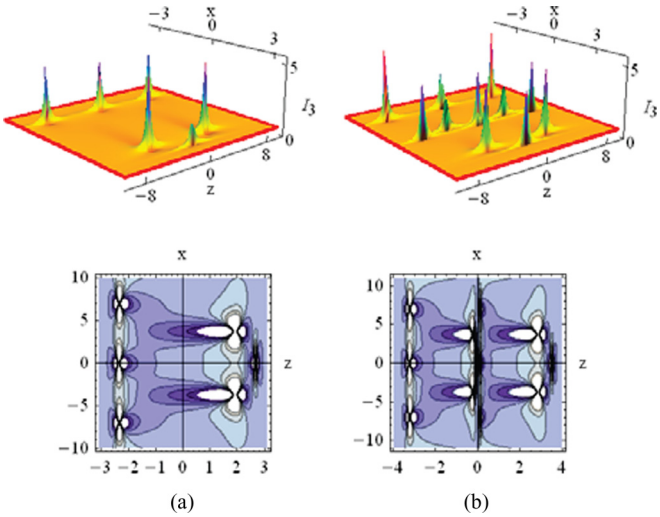

FIG. 6. (Color online) General third-order rogue waves with the parameters $\beta_1 = \beta_2 = 0$ and $\alpha_1 = \alpha_2 = 50$: (a) $m = 0$ and (b) $m = 1$. The setup is as in Fig. 5.

rogue wave with six high peaks. If a larger parameter m is selected, the structure of the rogue wave is significantly more complicated, as shown in Fig. 6(b) for $m = 1$.

Finally, we choose four parameters: $\alpha_1 = 0$, $\alpha_2 = 0$, $\beta_1 = 1$, and $\beta_2 = 5000$. To display the characteristics of this peculiar third-order solution of Eq. (7), the evolution of the rogue wave is plotted in Fig. 7. Complicated patterns are obtained.

E. Numerical simulation

In the end, we briefly test the stability of the rogue wave solutions found above. We take the fundamental third-order rogue wave solution (7) as an initial wave perturbed by a random noise to perform numerical simulation of Eq. (1) with a special external potential parameter $a = -1/4$. The simulations should also confirm the validity of analytical solutions

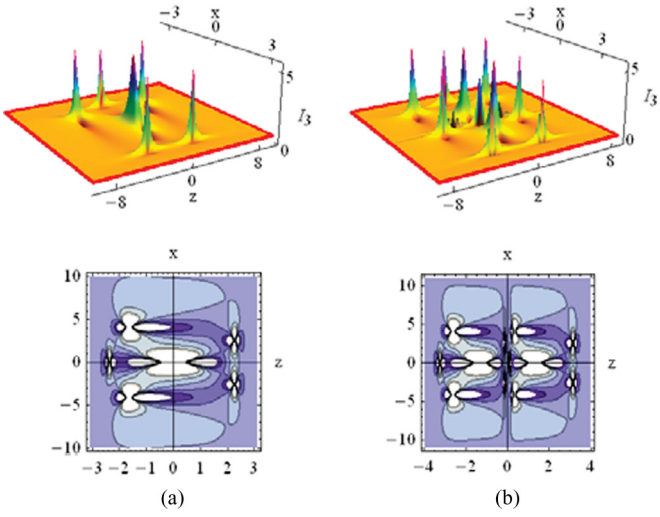

FIG. 7. (Color online) Intensities of the third-order solution of Eq. (7) with the parameters $\alpha_1 = 0$, $\alpha_2 = 0$, $\beta_1 = 1$, and $\beta_2 = 5000$: (a) $m = 0$ and (b) $m = 1$. The setup is as in Fig. 5.

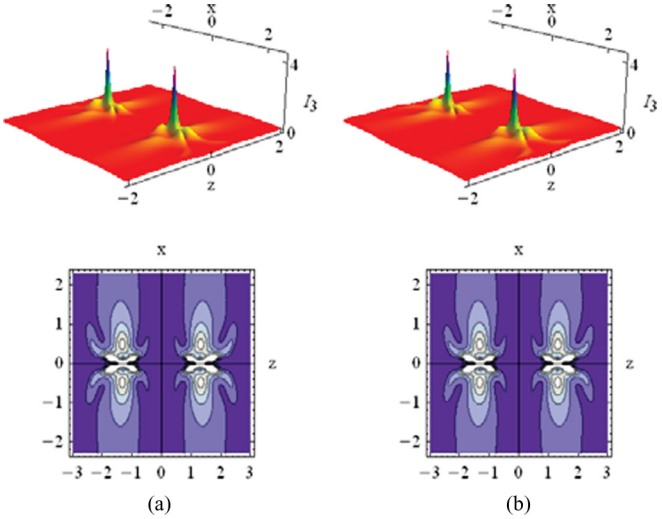

FIG. 8. (Color online) Comparison of the analytical solution with the numerical simulations for the fundamental third-order rogue waves at $z = 80$: (a) analytical solution of Eq. (7) and (b) numerical simulation of Eq. (1).

(7) by comparing them to their numerical counterparts. In order to do so, we add white noise to the initial pulse $u(0,x)$ in the amount of 5% amplitude random noise so that the perturbed pulse is written as $u_{\text{pert}} = u(0,x)[1 + 0.05\text{random}(x)]$. Figure 8 compares the analytical solution of Eq. (7) with the numerical simulation of Eq. (1) for $\alpha_1 = \beta_1 = 0$ by using the split-step beam-propagation method [34–36]. Here, we keep the same parameters as in Fig. 5, but the parabolic-cylinder order is chosen as $m = 1$. As expected, the rogue wave can propagate in a stable manner for a while under the initial perturbation of white noise and is in good agreement with the analytical solution. Although here we have demonstrated the results of the stability only for an example in Eq. (1), similar conclusions hold for other solution cases as well, provided propagation distances are kept within reasonable values. One should keep in mind that rogue waves riding on a finite background often suffer from modulational instabilities.

IV. CONCLUSIONS

In conclusion, we have presented analytical rogue wave solutions of the generalized NLSE with spatially modulated coefficients and a special external potential. By utilizing the similarity transformation, we have demonstrated that a class of parabolic-cylinder optical rogue waves can exist in specific inhomogeneous media. Our results show that these controllable patterns of the optical rogue waves can be realized by selecting different orders of the parabolic-cylinder function and of the basic rogue wave solutions of NLSE with constant coefficients. A numerical simulation is performed to compare with the analytical solution and to confirm the relative stability of localized solutions. Since the understanding of rogue waves is important in the (2+1)-dimensional models, which characterize the more realistic evolution in the transverse (x, y) plane, we plan to extend our study to multidimensional NLSE models.

ACKNOWLEDGMENTS

This work was supported by the National Natural Science Foundation of China under Grants No. 61275001 and No. 11474146. Work at the Texas A&M University at Qatar is supported by Project No. NPRP 6-021-1-005 with the Qatar National Research Fund (a member of the Qatar Foundation). Work in Serbia was done under Project No. OI 171006 of the Ministry of Education and Science of Serbia.

APPENDIX A: EXACT ROGUE WAVE SOLUTIONS

We use the direct integration method to obtain rogue wave solutions of Eq. (3). To find the first-order rogue wave solution, we assume the solution of Eq. (3) in the form

$$V_1(z,Y)=\left[-1+\frac{G_1(z,Y)+iH_1(z,Y)}{F_1(z,Y)}\right]e^{2iz}, \quad \text{(A1)}$$

with $G_1(z,Y)=g_0$, $H_1(z,Y)=h_0+h_1z+h_2Y$, $F_1(z,Y)=f_0+f_1z^2+f_2Y^2$, where g_j, h_j, and f_j $(j=0,1,2)$ are real constants and the factor e^{2iz} is a seed solution of Eq. (3). Substituting Eq. (A1) into Eq. (3) and setting all coefficients of $z^kY^j(k,j\geqslant 0)$ to zero, for $f_j\neq 0$ to avoid singularities in F_1, we obtain a system of algebraic equations, which are then solved, to obtain $g_0=1$, $h_0=0$, $h_1=4$, $h_2=0$, $f_0=1/4$, $f_1=4$, $f_2=1$, namely,

$$G_1(z,Y)=1, \quad H_1(z,Y)=4z, \quad F_1(z,Y)=\tfrac{1}{4}+4z^2+Y^2.$$

We further apply the direct method to find the second-order rogue wave solution as follows:

$$V_2(z,Y)=\left[1+\frac{G_2(z,Y)+iH_2(z,Y)}{F_2(z,Y)}\right]e^{2iz}, \quad \text{(A2)}$$

with

$$\begin{aligned}
G_2(z,Y)&=g_0+g_1z+g_2zY+g_3Y+g_4z^2+g_5z^2Y^2+g_6Y^2+g_7z^4+g_8Y^4,\\
H_2(z,Y)&=h_0+h_1z+h_2Y+h_3z^2+h_4zY+h_5Y^2+h_6z^5+h_7z^3+h_8zY^2+h_9z^3Y^2+h_{10}zY^2+h_{11}zY^4,\\
F_2(z,Y)&=f_0+f_1z+f_2Y+f_3z^2+f_4Y^2+f_5z^3+f_6zY^2+f_7z^2Y+f_8Y^3+f_9z^4+f_{10}z^2Y^2+f_{11}Y^4\\
&\quad+f_{12}z^6+f_{13}z^2Y^4+f_{14}z^4Y^2+f_{15}Y^6.
\end{aligned}$$

Again, substituting Eq. (A2) into Eq. (3) and using *Mathematica*, we obtain the following relations:

$$\begin{aligned}
&g_0=36, \quad g_1=-115\beta_1, \quad g_2=0, \quad g_3=-576\alpha_1, \quad g_4=-3456, \quad g_5=-4608, \quad g_6=-288,\\
&g_7=-15360, \quad g_8=-192;\\
&h_0=144\beta_1, \quad h_1=720, \quad h_2=0, \quad h_3=-2304\beta_1, \quad h_4=-2304\alpha_1, \quad h_5=576\beta_1, \quad h_6=-12288,\\
&h_7=-1636, \quad h_8=1152, \quad h_9=-6144, \quad h_{10}=1152, \quad h_{11}=-768;\\
&f_0=9+144\left({\alpha_1}^2+{\beta_1}^2\right), \quad f_1=864\beta_1, \quad f_2=144\alpha_1, \quad f_3=1584, \quad f_4=108, \quad f_5=1536\beta_1,\\
&f_6=-1152\beta_1, \quad f_7=2304\alpha_1, \quad f_8=-192\alpha_1, \quad f_9=6912, \quad f_{10}=-1152, \quad f_{11}=48, \quad f_{12}=4096,\\
&f_{13}=768, \quad f_{14}=3072, \quad f_{15}=64;
\end{aligned}$$

where α_1 and β_1 are two arbitrary real constants. Thus, $G_2(z,Y)$, $H_2(z,Y)$, and $F_2(z,Y)$ can be written as follows:

$$\begin{aligned}
G_2(z,Y)&=36-115\beta_1z-576\alpha_1Y-3456z^2-4608z^2Y^2-288Y^2-15\,360z^4-192Y^4,\\
H_2(z,Y)&=144\beta_1+720z-2304\beta_1z^2-2304\alpha_1zY+576\beta_1Y^2-12\,288z^5-1636z^3\\
&\quad+1152zY^2-6144z^3Y^2+1152zY^2-768zY^4,\\
F_2(z,Y)&=9+144\left({\alpha_1}^2+{\beta_1}^2\right)+864\beta_1z+144\alpha_1Y+1584z^2+108Y^2+1536\beta_1z^3-1152\beta_1zY^2\\
&\quad+2304\alpha_1z^2Y-192\alpha_1Y^3+6912z^4-1152z^2Y^2+48Y^4+4096z^6+768z^2Y^4+3072z^4Y^2+64Y^6.
\end{aligned}$$

In a similar procedure, we obtain the following third-order rogue wave solutions of Eq. (3):

$$V_3(z,Y)=\left[-1+\frac{G_3(z,Y)+iH_3(z,Y)}{F_3(z,Y)}\right]e^{2iz}. \quad \text{(A3)}$$

The expressions for G_3, H_3, and F_3 are given as follows:

$$G_3(z,Y)=16200+3600\left(\alpha_1^2+\beta_1^2\right)+144\left(\alpha_2^2+\beta_2^2\right)+G_3^{(1)}(Y)+\sum_{l=1}^{10}g_l(Y)z^l,$$

$$H_3(z,Y)=-16200\beta_1-2400\beta_1\left(\alpha_1^2+\beta_1^2\right)+960\alpha_1\alpha_2\beta_1-1080\beta_2+480\beta_2\left(\beta_1^2-\alpha_1^2\right)+H_3^{(1)}(Y)+\sum_{l=1}^{11}h_l(Y)z^l,$$

$$\begin{aligned}
F_3(z,Y)&=2025+2700\left(\alpha_1^2+\beta_1^2\right)+400\left(\alpha_1^4+\beta_1^4\right)+360\left(\alpha_1\alpha_2+\beta_1\beta_2\right)+36\left(\alpha_2^2+\beta_2^2\right)+800\alpha_1^2\beta_1^2\\
&\quad+F_3^{(0)}+F_3^{(1)}(Y)+\sum_{l=1}^{12}f_l(Y)z^l,
\end{aligned}$$

where

$$G_3^{(1)}(Y) = 24576Y^{10} + 92160Y^8 + 322560Y^6 + (230400\alpha_1 - 13824\alpha_2)\,Y^5 + \left(57600\alpha_1^2 - 19200\beta_1^2 - 172800\right)Y^4$$
$$- (115200\alpha_1 + 11520\alpha_2)Y^3 - \left(64800 + 28800\alpha_1^2 + 28800\beta_1^2\right)Y^2 - \left(43200\alpha_1 + 9600\alpha_1^3 + 4320\alpha_2 + 9600\alpha_1\beta_1^2\right)Y,$$

$$g_{10}(Y) = 276824064, \quad g_9(Y) = 0, \quad g_8(Y) = 283115520Y^2 + 778567680, \quad g_7(Y) = -47185920\beta_1,$$

$$g_6(Y) = 110100480Y^4 + 165150720Y^2 + 55050240\alpha_1 Y + 215285760,$$

$$g_5(Y) = -29491200\beta_1 - 1032192\beta_2,$$

$$g_4(Y) = 19660800Y^6 - 14745600Y^4 + 19660800\alpha_1 Y^3 + 165888000Y^2 + (1843200\alpha_2 - 25804800\alpha_1)\,Y$$
$$- 47001600 + 2150400\alpha_1^2 + 921600\beta_1^2,$$

$$g_3(Y) = 4915200\beta_1 Y^4 + (1105920\beta_2 - 36864000\beta_1)\,Y^2 + 2457600\alpha_1\beta_1 Y + 10137600\beta_1 - 645120\beta_2,$$

$$g_2(Y) = 1474560Y^8 - 1474560Y^6 + 1474560\alpha_1 Y^5 + 2764800Y^4 + (9216000\alpha_1 - 184320\alpha_2)\,Y^3$$
$$+ \left(1382400\beta_1^2 - 460800\alpha_1^2 - 20736000\right)Y^2$$
$$+ (414720\alpha_2 - 2764800\alpha_1)\,Y - 345600\alpha_1^2 + 46080\alpha_1\alpha_2 - 806400\beta_1^2 + 46080\beta_1\beta_2 - 777600,$$

$$g_1(Y) = 491520\beta_1 Y^6 + 46080\beta_2 z Y^4 - 614400\alpha_1\beta_1 Y^3 + (1382400\beta_1 + 69120\beta_2)\,Y^2$$
$$+ (23040\alpha_1\beta_2 - 23040\alpha_2\beta_1 + 230400\alpha_1\beta_2)Y + 19200\alpha_1^2\beta_1 + 19200\beta_1^3 - 8640\beta_2,$$

$$H_3^{(1)}(Y) = 30720\beta_1 Y^8 + (92160\beta_1 - 7680\beta_2)\,Y^6 + 30720\alpha_1\beta_1 Y^5 + (57600\beta_1 - 5760\beta_2)\,Y^4$$
$$+ (38400\alpha_1\beta_1 - 3840\alpha_2\beta_1 + 3840\alpha_1\beta_2)\,Y^3 - \left(86400\beta_1 + 9600\beta_1\alpha_1^2 + 9600\beta_1^3 + 12960\beta_2\right)Y^2$$
$$+ 2880\alpha_2\beta_1 Y - 2880\alpha_1\beta_2 Y,$$

$$h_{11}(Y) = 100663296, \quad h_{10}(Y) = 0, \quad h_9(Y) = 125829120Y^2 + 157286400, \quad h_8(Y) = -23592960\beta_1,$$

$$h_7(Y) = 62914560Y^4 - 94371840Y^2 + 31457280\alpha_1 Y - 342097920, \quad h_6(Y) = 3932160\beta_1 - 688128\beta_2,$$

$$h_5(Y) = 15728640Y^6 + 82575360Y^4 + 15728640\alpha_1 Y^3 + 168099840Y^2 + (1474560\alpha_2 - 56033280\alpha_1)\,Y$$
$$+ 1720320\alpha_1^2 + 737280\beta_1^2 - 236666880,$$

$$h_4(Y) = 4915200\beta_1 Y^4 + (1105920\beta_2 - 51609600\beta_1)\,Y^2 + 2457600\alpha_1\beta_1 Y + 35942400\beta_1 - 460800\beta_2,$$

$$h_3(Y) = 1966080Y^8 - 13762560Y^6 + 1966080\alpha_1 Y^5 - 11059200Y^4 + (12288000\alpha_1 - 245760\alpha_2)\,Y^3$$
$$+ \left(1843200\beta_1^2 - 38707200 - 614400\alpha_1^2\right)Y^2 + (184320\alpha_2 - 7372800\alpha_1)\,Y - 1382400\alpha_1^2 + 61440\alpha_1\alpha_2$$
$$-1996800\beta_1^2 + 61440\beta_1\beta_2 - 3801600,$$

$$h_2(Y) = 983040\beta_1 Y^6 + 92160\beta_2 Y^4 - 1228800\alpha_1\beta_1 Y^3 + (2764800\beta_1 - 138240\beta_2)\,Y^2 + (460800\alpha_1\beta_1 - 46080\alpha_2\beta_1$$
$$+ 46080\alpha_1\beta_2)Y + 38400\beta_1\alpha_1^2 + 38400\beta_1^3 + 190080\beta_2,$$

$$h_1(Y) = 98304Y^{10} - 368640Y^8 - 921600Y^6 + 184320\alpha_1 Y^5 - 55296\alpha_2 Y^5 + \left(230400\alpha_1^2 - 76800\beta_1^2 - 2073600\right)Y^4$$
$$+ (46080\alpha_2 - 1382400\alpha_1)\,Y^3 + \left(115200\alpha_1^2 + 115200\beta_1^2 + 1814400\right)Y^2 - \left(172800\alpha_1 + 38400\alpha_1^3 + 86400\alpha_2\right.$$
$$\left. + 38400\alpha_1\beta_1^2\right)Y + 72000\alpha_1^2 - 23040\alpha_1\alpha_2 + 576\alpha_2^2 + 72000\beta_1^2 - 23040\beta_1\beta_2 + 576\beta_2^2 + 453600,$$

$$F_3^{(1)}(Y) = 4096Y^{12} + 6144Y^{10} - 10240\alpha_1 Y^9 + 34560Y^8 + (1536\alpha_2 - 15360\alpha_1)\,Y^7 + \left(8960\beta_1^2 + 3840\alpha_1^2 + 149760\right)Y^6$$
$$+ (69120\alpha_1 - 3456\alpha_2)\,Y^5 + \left(33600\alpha_1^2 - 1920\alpha_1\alpha_2 + 14400\beta_1^2 - 1920\beta_1\beta_2 + 54000\right)Y^4 + (3200\alpha_1\beta_1^2 - 14400\alpha_1$$
$$+ 3200\alpha_1^3 - 4320\alpha_2)Y^3 + \left(144\beta_2^2 + 3600\alpha_1^2 - 28800\alpha_1\alpha_2 + 144\alpha_2^2 + 3600\beta_1^2 - 2880\beta_1\beta_2 + 48600\right)Y^2$$
$$+ \left(16200\alpha_1 + 2400\alpha_1^3 + 1080\alpha_2 - 480\alpha_1^2\alpha_2 + 2400\alpha_1\beta_1^2 + 480\alpha_2\beta_1^2 - 960\alpha_1\beta_1\beta_2\right)Y,$$

$$F_3^{(0)} = -55115529584640\beta_1 + 35055206400\beta_1\alpha_1^2 - 491520000\alpha_1^4\beta_1 - 4600627200\alpha_1\alpha_2\beta_1 + 196608000\alpha_1^3\alpha_2\beta_1$$
$$+ 1730740224000\beta_1^3 - 6881280000\alpha_1^2\beta_1^3 + 196608000\alpha_1\alpha_2\beta_1^3 - 6389760000\beta_1 + 317973921792\beta_2$$
$$- 66355200\alpha_1^2\beta_2 + 265420800\alpha_1\alpha_2\beta_2 - 54632448000\beta_1^2\beta_2$$
$$+ 196608000\alpha_1^2\beta_1^2\beta_2 + 196608000\beta_1^4\beta_2 + 265420800\beta_1\beta_2^2,$$

$$f_{12}(Y) = 16777216, \quad f_{11}(Y) = 0, \quad f_{10}(Y) = 25165824Y^2 + 132120576, \quad f_9(Y) = -5242880\beta_1,$$

$$f_8(Y) = 15728640Y^4 + 70778880Y^2 + 7864320\alpha_1 Y + 244776960, \quad f_7(Y) = 0,$$

$$f_6(Y) = 5242880Y^6 + 3932160Y^4 + 5242880\alpha_1 Y^3 + 221184000Y^2 + (491520\alpha_2 - 2949120\alpha_1)\,Y + 573440\alpha_1^2 + 245760\beta_1^2 + 62668800,$$

$$f_5(Y) = 1966080\beta_1 Y^4 + (442368\beta_2 - 26542080\beta_1)\,Y^2 + 983040\alpha_1\beta_1 Y + 7004160\beta_1 - 626688\beta_2,$$

$$f_4(Y) = 983040Y^8 - 2949120Y^6 + 983040\alpha_1 Y^5 - 5529600Y^4 + (15974400\alpha_1 - 122880\alpha_2)\,Y^3 + \left(921600\beta_1^2 - 307200\alpha_1^2 + 80179200\right)Y^2 + (829440\alpha_2 - 11059200\alpha_1)\,Y + 3840,$$

$$f_3(Y) = 655360\beta_1 Y^6 + (61440\beta_2 + 2457600\beta_1)\,Y^4 - 819200\alpha_1\beta_1 Y^3 + (276480\beta_2 - 16588800\beta_1)Y^2 + (1536000\alpha_1\beta_1 - 30720\alpha_2\beta_1 + 30720\alpha_1\beta_2)Y,$$

$$f_2(Y) = 98304Y^{10} - 368640Y^8 + 552960Y^6 + (184320\alpha_1 - 55296\alpha_2)\,Y^5 + \left(230400\alpha_1^2 - 76800\beta_1^2 + 3456000\right)Y^4 + (2304000\alpha_1 + 46080\alpha_2)\,Y^3 + \left(1036800\beta_1^2 + 115200\alpha_1^2 - 2332800\right)Y^2 + \left(190080\alpha_2 - 172800\alpha_1 - 38400\alpha_1^3 - 38400\alpha_1\beta_1^2\right)Y + 302400\alpha_1^2 - 23040\alpha_1\alpha_2 + 576\beta_2^2 + 576\alpha_2^2 + 532800\beta_1^2 - 23040\beta_1\beta_2 + 1490400,$$

$$f_1(Y) = 61440\beta_1 Y^8 + (61440\beta_1 - 15360\beta_2)\,Y^6 + (34560\beta_2 - 284160\alpha_1\beta_1)\,Y^4 + (7680\alpha_1\beta_2 - 7680\alpha_2\beta_1 - 230400\alpha_1\beta_1)\,Y^3 + \left(172800\beta_1 - 19200\alpha_1^2\beta_1 - 19200\beta_1^3 + 43200\beta_2\right)Y^2 + (17280\alpha_1\beta_2 - 17280\alpha_2\beta_1)\,Y - 118800\beta_1 - 24000\beta_1\alpha_1^2 + 1920\alpha_1\alpha_2\beta_1 - 24000\beta_1^3 - 10800\beta_2 - 960\alpha_1^2\beta_2 + 960\beta_1^2\beta_2.$$

It should be emphasized that the first-order rogue wave solution has no free parameters, the second-order rogue wave solution has a pair of free parameters (two real numbers: α_1 and β_1), while the third-order rogue wave solution has two pairs of free parameters (four real numbers: α_1, β_1, α_2, and β_2).

APPENDIX B: THE RELATION BETWEEN PARABOLIC-CYLINDER AND CONFLUENT HYPERGEOMETRIC FUNCTION

The parabolic-cylinder differential equation (PCDE) has two standard forms:

$$\frac{d^2y}{dx^2} - \left(\frac{1}{4}x^2 + \Omega\right)y = 0, \tag{B1}$$

$$\frac{d^2y}{dx^2} + \left(\frac{1}{4}x^2 - \Omega\right)y = 0. \tag{B2}$$

For a general Ω, the even and odd solutions to (B1) and (B2) are

$$y_1(x) = e^{-\frac{1}{4}x^2}\,{}_1F_1\left(\frac{1}{2}\Omega + \frac{1}{4}; \frac{1}{2}; \frac{1}{2}x^2\right), \tag{B3}$$

$$y_2(x) = xe^{-\frac{1}{4}x^2}\,{}_1F_1\left(\frac{1}{2}\Omega + \frac{3}{4}; \frac{3}{2}; \frac{1}{2}x^2\right), \tag{B4}$$

where ${}_1F_1$ is a confluent hypergeometric function. When $\Omega = m + \frac{1}{2}$, from (B3) we easily find

$$D_m(x) = e^{-\frac{1}{4}x^2}\,{}_1F_1\left(\frac{m+1}{2}; \frac{1}{2}; \frac{1}{2}x^2\right), \tag{B5}$$

$$D_{-m-1}(ix) = e^{\frac{1}{4}x^2}\,{}_1F_1\left(-\frac{m}{2}; \frac{1}{2}; -\frac{1}{2}x^2\right), \tag{B6}$$

both functions being real. Thus Eq. (6d) can be simplified as

$$A(x) = \sqrt{\frac{1}{\sqrt{2\pi}m!}}\left[c_1 e^{-\frac{1}{4}x^2}\,{}_1F_1\left(\frac{m+1}{2}; \frac{1}{2}; \frac{1}{2}x^2\right) + c_2 e^{\frac{1}{4}x^2}\,{}_1F_1\left(-\frac{m}{2}; \frac{1}{2}; -\frac{1}{2}x^2\right)\right].$$

[1] N. Akhmediev, A. Ankiewicz, and M. Taki, Phys. Lett. A **373**, 675 (2009).
[2] N. Akhmediev, A. Ankiewicz, and J. M. Soto-Crespo, Phys. Rev. E **80**, 026601 (2009).
[3] K. Hammani, B. Kibler, C. Finot, P. Morin, J. Fatome, J. M. Dudley, and G. Milot, Opt. Lett. **36**, 112 (2011).
[4] L. Wen, L. Li, Z. D. Li, S. W. Song, X. F. Zhang, and W. M. Liu, Eur. Phys. J. D **64**, 473 (2011).
[5] A. Chabchoub, N. P. Hoffmann, and N. Akhmediev, Phys. Rev. Lett. **106**, 204502 (2011).
[6] H. Bailung, S. K. Sharma, and Y. Nakamura, Phys. Rev. Lett. **107**, 255005 (2011).
[7] L. Berge, Phys. Plasmas **4**, 1227 (1997).
[8] L. Berge, V. K. Mezentsev, J. J. Rasmussen, P. L. Christiansen, and Yu. B. Gaididei, Opt. Lett. **25**, 1037 (2000).
[9] T. J. Alexander and L. Berge, Phys. Rev. E **65**, 026611 (2002).
[10] C. Kharif, E. Pelinovsky, and A. Slunyacv, *Rogue Waves in the Ocean, Theories and Modeling* (Springer-Verlag, New York, 2009).
[11] D. R. Solli, C. Ropers, P. Koonath, and B. Jalali, Nature (London) **450**, 1054 (2007).
[12] M. Onorato, S. Residori, U. Bortolozzo, A. Montinad, and F. T. Arecchi, Phys. Rep. **528**, 47 (2013).

[13] N. Akhmediev, J. M. Dudley, D. R. Solli, and S. K. Turitsyn, J. Opt. **15**, 060201 (2013).
[14] D. H. Peregrine, J. Austral. Math. Soc. Ser. B **25**, 16 (1983).
[15] Y. C. Ma, Stud. Appl. Math. **60**, 43 (1979).
[16] N. Akhmediev, V. M. Eleonskii, and N. Kulagin, Zh. Eksp. Teor. Fiz. **89**, 1542 (1985).
[17] N. Akhmediev and V. I. Korneev, Theor. Math. Phys. **69**, 1089 (1986).
[18] A. Chabchoub, N. P. Hoffmann, M. Onorato, and N. Akhmediev, Phys. Rev. X **2**, 011015 (2012).
[19] A. Chabchoub, N. Hoffmann, M. Onorato, A. Slunyaev, A. Sergeeva, E. Pelinovsky, and N. Akhmediev, Phys. Rev. E **86**, 056601 (2012).
[20] M. Erkintalo, K. Hammani, B. Kibler, C. Finot, N. Akhmediev, J. M. Dudley, and G. Genty, Phys. Rev. Lett. **107**, 253901 (2011).
[21] P. Shukla and W. Moslem, Phys. Lett. A **376**, 1125 (2012).
[22] R. Sabry, W. M. Moslem, and P. K. Shukla, Phys. Rev. E **86**, 036408 (2012).
[23] L. Ling and L.-C. Zhao, Phys. Rev. E **88**, 043201 (2013).
[24] W. P. Zhong, M. R. Belić, and T. Huang, Phys. Rev. E **87**, 065201 (2013); W. P. Zhong, J. Nonlinear Opt. Phys. Mater. **21**, 1250026 (2012).
[25] W. P. Zhong and M. R. Belić, Phys. Rev. E **81**, 056604 (2010).
[26] M. Belic and W. P. Zhong, Eur. Phys. J. D **53**, 97 (2009).
[27] W. P. Zhong and M. Belic, Phys. Lett. A **373**, 296 (2009).
[28] D. Zwillinger, *Handbook of Differential Equations*, 3rd ed. (Academic Press, Boston, 1997).
[29] J. R. Tayor, *Optical Solitons—Theory and Experiment* (Cambridge University Press, Cambridge, UK, 1992).
[30] P. G. Kevrekidis, D. J. Frantzeskakis, and R. Carretero-Gonzales, *Emergent Nonlinear Phenomena in BECs: Theory and Experiment* (Springer, Berlin, 2007).
[31] R. Carretero-Gonzales, D. J. Frantzeskakis, and P. G. Kevrekidis, Nonlinearity **21**, R139 (2008).
[32] Y. S. Kivshar and G. Agrawal, *Optical Solitons: From Fibers to Photonic Crystals* (Academic Press, London, 2003).
[33] S. A. Morgan, R. J. Ballagh, and K. Burnett, Phys. Rev. A **55**, 4338 (1997).
[34] M. Belić, N. Petrović, W. P. Zhong, R.-H. Xie, and G. Chen, Phys. Rev. Lett. **101**, 123904 (2008).
[35] E. A. Sziklas and A. E. Siegman, Appl. Opt. **14**, 1874 (1975).
[36] W. P. Zhong, M. R. Belić, G. Assanto, B. A. Malomed, and T. Huang, Phys. Rev. A **83**, 043833 (2011).